Progress In Electromagnetics Research Letters, Vol. 131, 26–33, 2026

PIER Letters

(Received 18 April 2026, Accepted 1 July 2026, Scheduled 11 July 2026)

Front-to-Back Ratio Improvement of Wideband Circularly Polarized Antenna with Tilted-Slot Fences

Bei-Wen Lin[1], Tian-Yuan Gao[1], and Rui Wu[1,2,*]

[1]*School of Integrated Circuits, Guangdong University of Technology, Guangzhou 510006, China*
[2]*State Key Laboratory of Millimeter Waves, Nanjing 210096, China*

ABSTRACT: This paper presents a wideband circularly polarized (CP) antenna featuring a significantly enhanced front-to-back ratio (FBR). The proposed design employs a composite structure that integrates a dipole with a loop resonator and is fabricated using a multilayer architecture. The top layer is a dielectric substrate loaded with a cyclic zigzag patch. The middle layer contains an L-shaped radiating patch with etched rectangular grooves, and the bottom layer comprises a metal ground plane and surrounding vertically tilted-slot fences. Circular polarization is achieved by exciting orthogonal degenerate modes via strategic rectangular-groove perturbations that work in concert with the loop resonator's inherent asymmetric current path. The tilted-slot fences, in conjunction with the zigzag patch layer, function collectively to suppress backward radiation and improve the FBR. Measured results demonstrate that the antenna achieves a 3 dB axial ratio (AR) bandwidth of 54% from 2.45 to 4.3 GHz, a stable FBR of more than 27.5 dB with 2.5 dB variation, and a peak gain of 9.3 dBic. This design offers a high-performance, planar antenna solution well-suited for satellite communication and radar systems.

1. INTRODUCTION

Circularly polarized antennas are widely used in satellite communication, radar detection, and navigation systems due to their advantages in alleviating polarization mismatch and suppressing multipath effects [1–4]. However, traditional circularly polarized antennas often sacrifice the key indicator of front-to-back ratio when pursuing wide-bandwidth beam performance [5–9]. For example, a crossover dipole with integrated phase delay was proposed in [5], which has a simple antenna structure and a 3 dB axial ratio of more than 15%. To improve bandwidth, a parasitic patch is introduced to achieve an axial-ratio bandwidth [6]. The dipole was designed as a rectangle, and the bandwidth of AR < 3 dB reaches 27% [7]. The front-to-back ratio (FBR) is about 15 dB in [5] and [6] and about 10 dB in [7]. The FBR of microstrip antennas is generally less than 15 dB when achieving a wide beam, while four-arm spiral antennas can improve the axial ratio but have a large size [10–12]. The prior antennas mainly improve FBR through the following ways [13–23]: by loading an electromagnetic bandgap structure [13], by setting up a long metasurface around the cross dipole [14], and by loading a ring on a resonant reflector antenna to form a butterfly antenna based on a resonant reflector [15]. By loading a circular aperture on the reflector, the current distribution on the reflector is changed, which effectively reduces the backward radiation of the antenna and improves the back-to-back ratio, and at the same time, the circular aperture has the effect of stabilizing the gain [16]. The design of the antenna itself and the addition of edge structures can also improve FBR, such as the semi-cylindrical sidewall structure on the reflector [17] and the composite cavity design around the antenna [18]. The two filtering CP antennas in [24, 25] suffer from insufficient FBR.

A prevalent bottleneck in current research is that most efforts are predominantly focused on bandwidth extension or gain enhancement. There remains a scarcity of systematic studies dedicated to improving the FBR of CP antennas. In particular, the potential of fence loading techniques for suppressing edge diffraction and optimizing FBR has not been fully exploited. This paper presents a novel design of tilted-slot fences. The synergistic design achieves a high FBR exceeding 25 dB while maintaining wideband circular polarization characteristics.

The remainder of this paper is organized as follows. Section 2 details the antenna configuration and provides an in-depth analysis of the design principles, including the circular-polarization generation mechanism and FBR enhancement strategy. Section 3 presents and discusses the simulated and measured results, validating the design. Finally, Section 4 concludes the paper.

2. ANTENNA CONFIGURATION AND DESIGN

The structure of the proposed antenna is illustrated in Fig. 1. The overall design leverages a combination of driven elements, parasitic components, and a reflector with backward radiation suppression function structures to achieve its performance goals. The antenna is excited by a coaxial probe located at the center of the structure. Energy is coupled to a pair of orthogonal dipoles through a quarter-wavelength delay ring printed on the substrate. This feeding configuration generates two orthogonal current modes with nearly equal amplitudes and a 90° phase difference, which is the fundamental condition for circular polarization radiation.

* Corresponding author: Rui Wu (wurui@gdut.edu.cn).

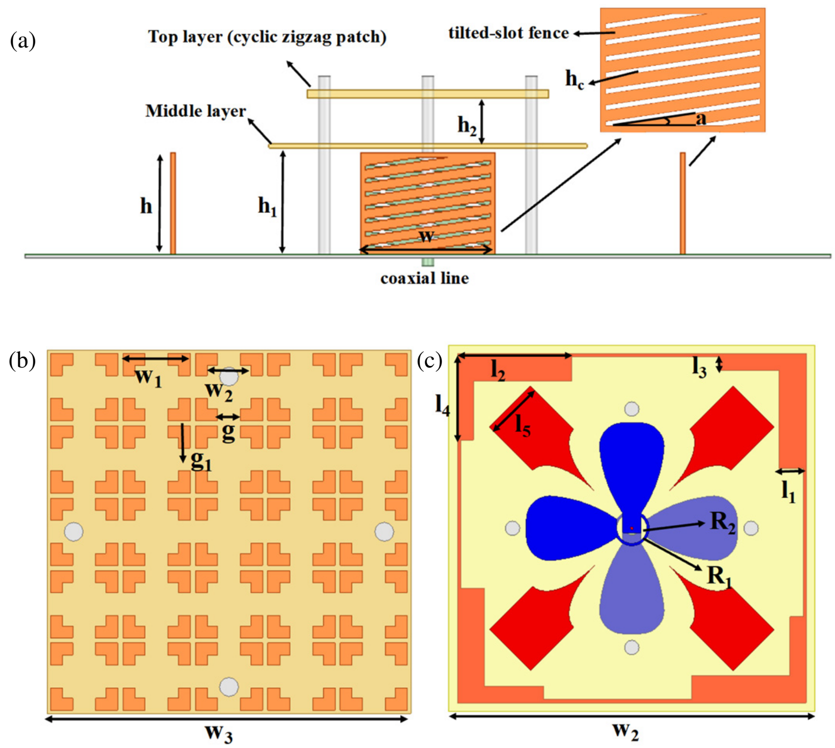

FIGURE 1. Antenna configurations. (a) Side view. (b) Top layer (cyclic zigzag patch). (c) Middle layer.

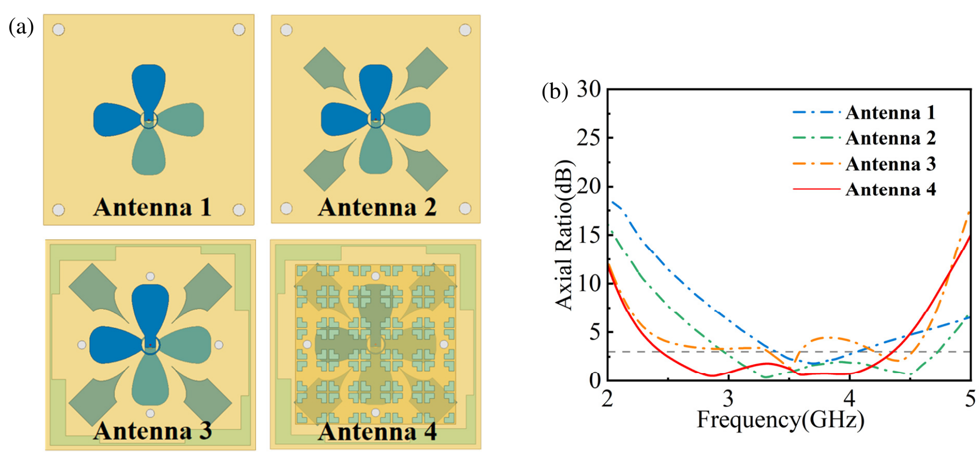

FIGURE 2. Design processor of the proposed antenna. (a) Reference antennas and proposed antenna and (b) axial ratio of the four antennas.

The primary radiating element is a modified loop resonator located on the middle layer ($\varepsilon_r = 4.4$, with a thickness of 0.8 mm). This patch is fed by a crossed-dipole structure via a 90° phase-shift feeding network to initiate circular polarization. Rectangular grooves are etched symmetrically onto the loop resonator to fine-tune the orthogonal modes. The top layer ($\varepsilon_r = 4.4$, with a thickness of 0.8 mm) is loaded with a parasitic cyclic zigzag patch, which serves to further optimize the axial ratio bandwidth. The bottom layer consists of a full metal ground plane and vertically oriented metallized sidewalls that surround the antenna structure. These sidewalls are not plain; their inner surfaces incorporate periodically arranged tilted slots, forming what we refer to as tilted slot fences. The sidewall height (h) is a critical parameter for FBR optimization. The antenna is built on an overall substrate with a larger footprint and a thickness of 1.6 mm.

2.1. Design of CP Antenna

To systematically illustrate the progressive enhancement of the axial-ratio bandwidth during the design process, four antenna configurations with increasing complexity are defined. As shown in Fig. 2(a), Antenna 4 is the final proposed antenna, which includes both a zigzag patch and tilted slot fences on the sidewalls. Fig. 2(b) presents the simulated AR of these four antennas over the 2–5 GHz frequency range. The AR values clearly demonstrate a progressive improvement from Antenna 1 to Antenna 4. After loading the zigzag patch, the AR is significantly reduced, confirming the phase-compensation effect of

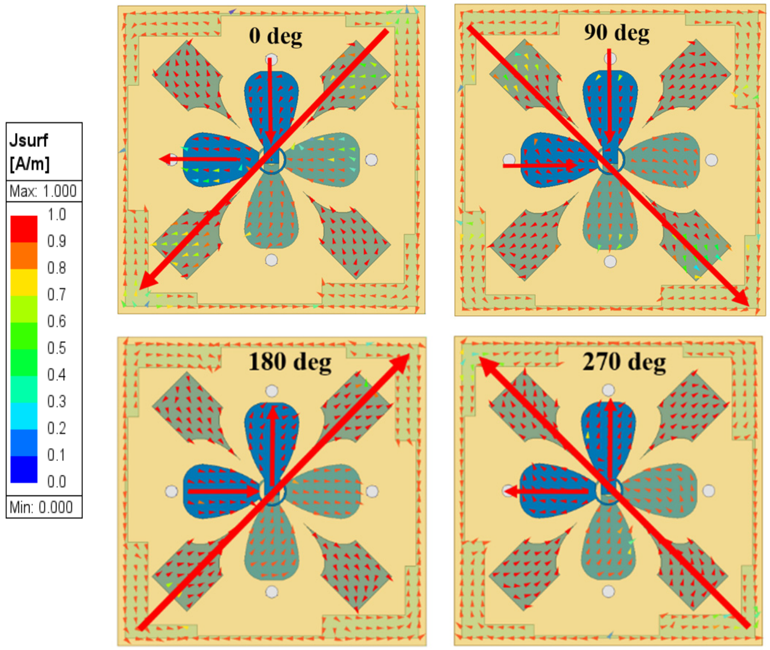

FIGURE 3. The current pattern of the antenna at 3.5 GHz.

the anisotropic zigzag structure. This evolutionary comparison validates that the synergistic integration of the zigzag patch and tilted slot fences is essential for achieving wideband circular polarization.

The fundamental principle for achieving circular polarization involves generating two orthogonal electric field components with equal amplitude and a 90° phase difference. In this design, the initial quadrature phase excitation is provided by the 90° phase-shift feed network, which excites the crossed dipole arms. This feed system induces currents on the primary loop resonator.

The rectangular grooves etched onto the loop resonator act as strategic disturbances to the surface current flow. These perturbations effectively modify the effective electrical length for currents flowing along different paths on the patch. By carefully optimizing the position and dimensions of these grooves, we can control the phase velocity of the two fundamental orthogonal modes, splitting their degenerate frequencies and creating the necessary 90° phase shift between them over a wide frequency band. This process, known as generating orthogonal degenerate modes, is crucial for wideband CP operation. The inherent geometric asymmetry of the loop resonator further helps create asymmetric current paths, which complements the action of the grooves to stabilize the CP performance. Fig. 3 shows the simulated surface current distribution on the antenna at 3.5 GHz and four different time phases (0°, 90°, 180°, 270°). The current vector clearly rotates clockwise, visually confirming the generation of right-hand circular polarization (RHCP).

To further broaden the 3 dB AR bandwidth, a parasitic cyclic zigzag patch is placed on the top substrate layer. This zigzag structure possesses anisotropic dielectric properties, which can be utilized to manipulate the wave impedance and phase response seen by the radiating fields from the primary loop resonator. It functions as a phase-compensating layer. At higher frequencies within the band, where phase errors typically degrade the AR, the zigzag patch introduces a compensating phase advance or delay, effectively correcting the phase relationship between the orthogonal modes across a broader spectrum. The simulated comparison in Fig. 4 demonstrates the significant effect of this parasitic element: after loading the zigzag patch, the 3 dB AR bandwidth is expanded substantially to 54.8%.

2.2. Mechanisms of Enhanced FBR

In this work, FBR is defined as the ratio of the peak gain in the main radiation direction (boresight, $\theta = 0°$) to the maximum gain within a specified angle of $\theta = 180°$ in the rear hemisphere. The FBR enhancement is primarily accomplished through the strategic use of the metallized sidewalls. These sidewalls serve two primary functions: forming a semi-enclosed cavity and suppressing surface waves. When designing the sidewall height, $h = \lambda/4$ (λ is the free space wavelength), the backward electric field E_{bk} and forward electric field E_{fd} are satisfied in (1):

$$|E_{bk}| = \left|\Gamma E_{fd} e^{-j2\beta h\_cebi}\right| \leq 0.056\,|E_{fd}| \tag{1}$$

(corresponding to the 25 dB front-to-back ratio), and the design takes $h = 20\,\text{mm}$ ($\lambda/5$).

Firstly, the sidewalls, together with the ground plane, create a shallow, semi-enclosed cavity. This cavity confines the radiated fields and significantly alters the edge-diffraction behavior of the antenna. Without sidewalls, significant currents can diffract over the edges of the ground plane, contributing to strong backward radiation. The vertical sidewalls redirect these edge-diffracted currents, converting them into in-phase reflections that contribute constructively to the forward radiation and destructively to the backward radiation. The height of the sidewall is a key parameter in this mechanism. As depicted

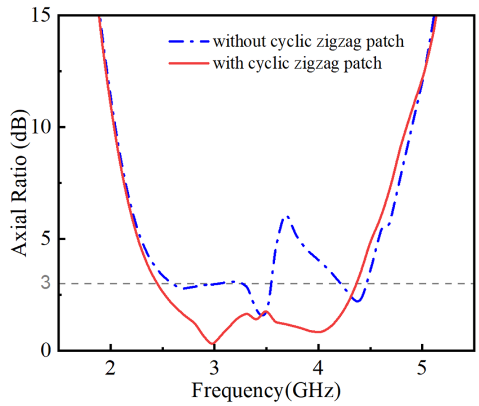

FIGURE 4. Effect of cyclic zigzag patch on AR of the antenna.

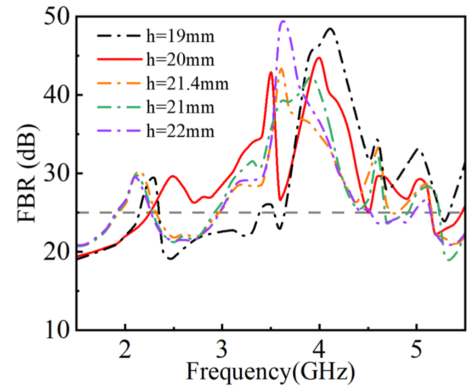

FIGURE 5. Effects of the height of the sidewall on FBR of the proposed antenna.

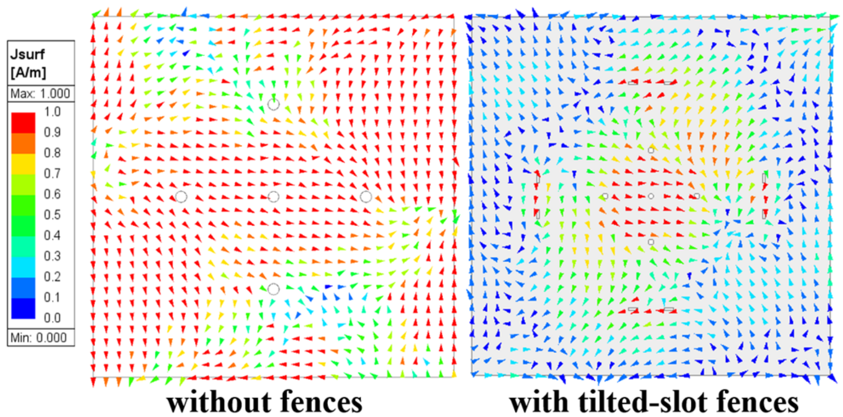

FIGURE 6. Effect of tilted-slot fences on current distribution of the antenna reflector.

clearly in Fig. 5, when h is approximately $\lambda/4$, the phase of the wave reflected from the sidewall's top edge can be optimized to achieve maximum cancellation of the backward wave. Our analysis determined that a height of $h = 20\,\text{mm}$ ($\approx \lambda/5$ at $\sim$3 GHz) provides an optimal compromise, theoretically satisfying the condition for significant backward wave cancellation and corresponding to an FBR improvement of around 25 dB, as suggested by Equation (1) in the original manuscript. Simulations confirm that increasing h from 0 to $\lambda/5$ reduces the backward radiation intensity by over 12 dB.

Secondly, the inner surfaces of the sidewalls are etched with a periodic array of tilted rectangular slots, forming tilted slot fences. These fences act as an impedance-modulated surface that helps to suppress the propagation of surface waves along the dielectric substrates. Surface waves, if unchecked, can travel to the edges of the antenna structure and radiate spuriously, often in the backward direction, thereby degrading the FBR. The periodic nature and specific tilted angle (a) of these slots are designed to create a stopband for these surface waves within the operating band. The tilt angle introduces asymmetry and coupling that enhances the surface-wave suppression capability.

Figure 6 shows the simulated current distribution on the ground plane and sidewalls at 3.5 GHz. It is observed that the current is predominantly concentrated near the center of the ground plane, directly beneath the driven patch, while the currents at the outer edges of the ground plane are markedly weaker. This current concentration indicates that the sidewalls effectively prevent energy from reaching and diffracting from the ground plane edges, which is a primary source of backward radiation.

Figure 7(a) compares the simulated FBR performance of three configurations: the original antenna without fences, the antenna with plain vertical fences, and the antenna with the proposed tilted-slot fences. The results clearly show the progressive improvement offered by each stage. The plain sidewalls provide a major boost, while the addition of the tilted slots offers a further refinement, ensuring that the FBR remains above 25 dB across the entire operating band. Fig. 7(b) illustrates the sensitivity of the FBR to the tilted angle a of the slots. After a parametric study, an optimal angle of $a = 8.3°$ was selected to maximize the FBR bandwidth and stability.

3. RESULTS AND ANALYSIS

A prototype of the proposed antenna was fabricated and measured to validate the proposed design. The photos from different perspectives of the proposed antenna are shown in Fig. 8.

The simulated and measured S parameters and ARs are depicted in Fig. 9(a). The simulated 10 dB impedance bandwidth

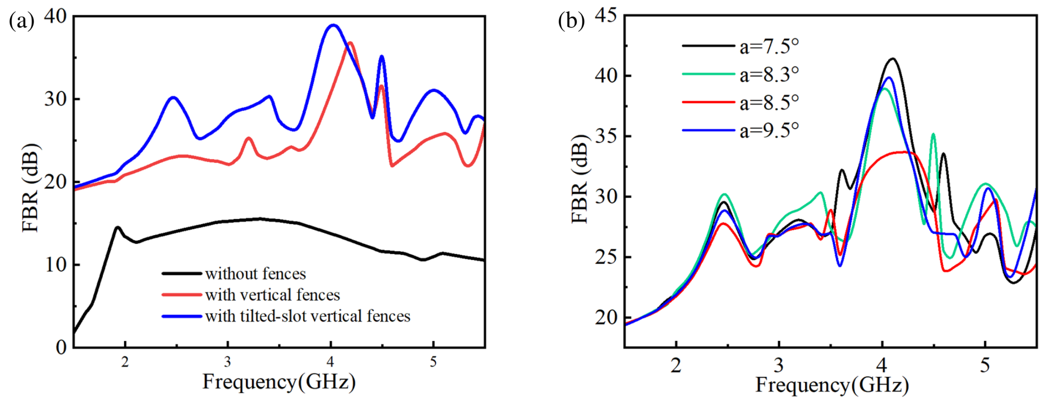

FIGURE 7. Key points of enhanced FBR. (a) Effects of fences and (b) effects of tilted angle (a).

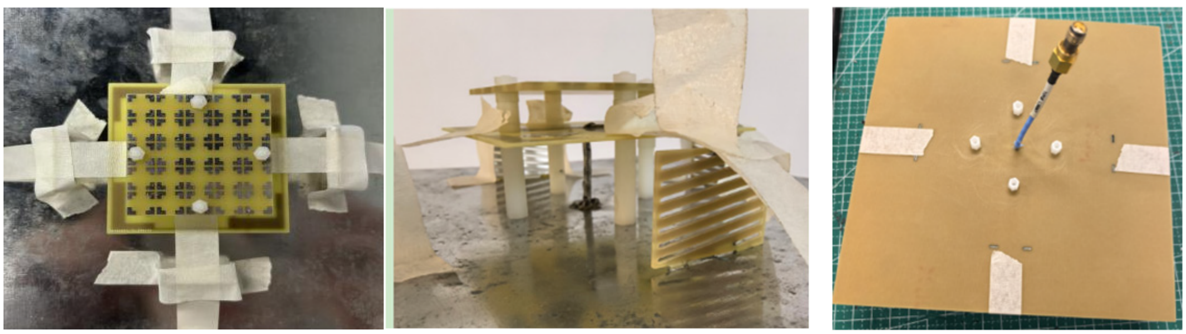

FIGURE 8. Photos of the proposed antenna.

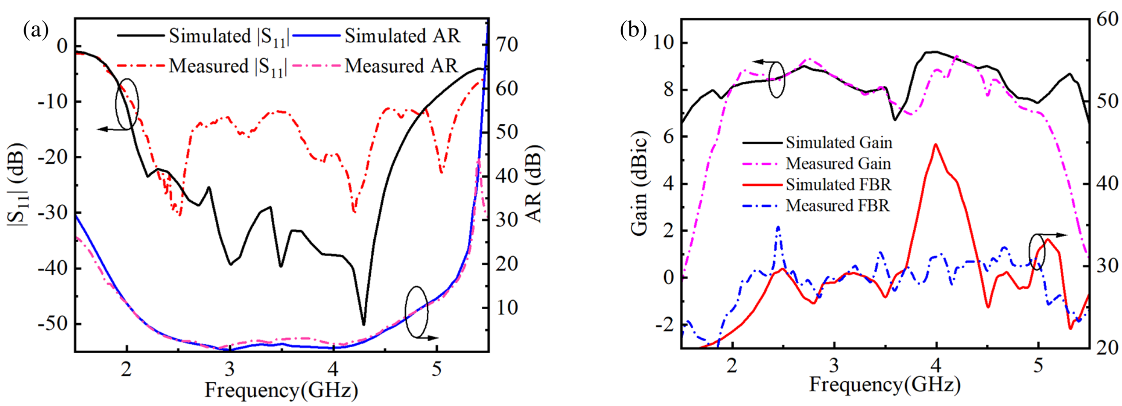

FIGURE 9. Simulated and measured results of (a) $|S_{11}|$ and AR, (b) FTB and gain.

ranges from 1.99 to 5.0 GHz (86%), while the measured result covers 1.99 to 4.96 GHz (85.5%), showing excellent agreement. For circular polarization, the simulated 3 dB AR bandwidth is 2.5–4.35 GHz (54%), and the measured result is 2.45–4.3 GHz (54%). The slight discrepancies between simulation and measurement are generally attributed to fabrication tolerances. In particular, manual positioning accuracy, including the spacing and position deviations between the dielectric boards, and the vertical tilt and positional errors of the tilted-slot fences, along with the soldering effects of the SMA connector, all affect the impedance characteristics of the antenna, thereby introducing reasonable additional ripples in the measured $|S_{11}|$ response within the mid-band region.

Figure 9(b) presents the simulated and measured FBRs and peak gains. A remarkable improvement in FBR is confirmed. The measured FBR is stable and maintained between 25 dB and 30 dB over the entire 2$\sim$5 GHz frequency range, which is more than double the FBR of the reference antenna without optimized sidewalls. The measured gain is stable, with a fluctuation of less than 1.4 dB within the CP band. The peak gain reaches 9.4 dBic at 4.2 GHz, and the gain remains above 7 dBi throughout the operating band. The radiation efficiency, derived from

TABLE 1. Comparison with reported CP antennas.

Ref.	3 dB AR Bandwidth	FBR (dB)	Peak Gain (dBi)	Impedance Bandwidth
[6]	28.6% 2.25–3 GHz	∼15	8.7	38.2% 1.97–2.9 GHz
[7]	27% 2.3–2.9 GHz	∼10	6.2	50.2% 1.99–3.22 GHz
[22]	25.9% 3.3–4.28 GHz	∼10	5.71	18.2% 2.14–2.57 GHz
[23]	30% 3.7–5.0 GHz	∼20	8	31.1% 3.8–5.2 GHz
[24]	51.2% 3.15–5.32 GHz	∼16	7.8	64.2% 2.88–5.63 GHz
[25]	44.2% 1.5–2.35 GHz	∼17	7.4	46.3% 1.67–2.71 GHz
This work	**54% 2.45–4.3 GHz**	**∼27.5**	**9.3**	**85.5% 1.99–4.96 GHz**

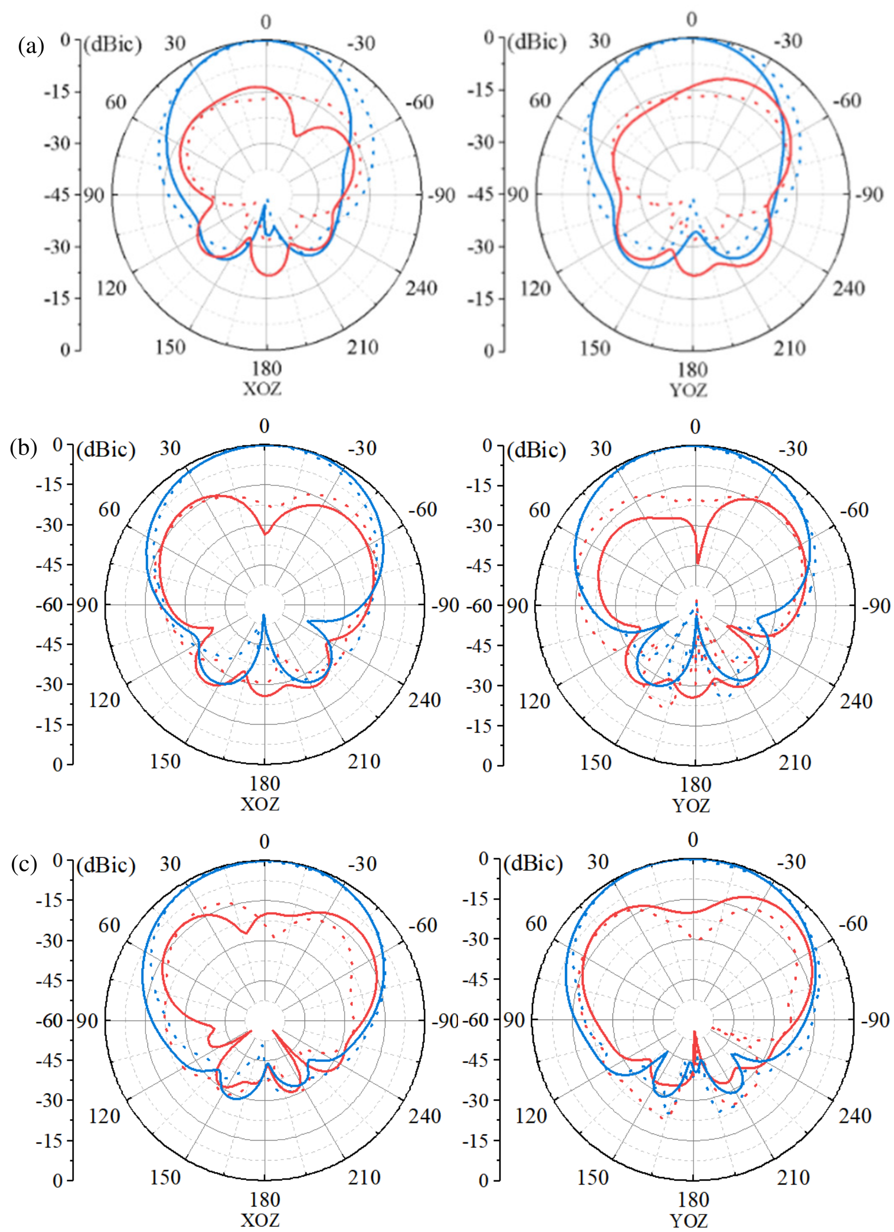

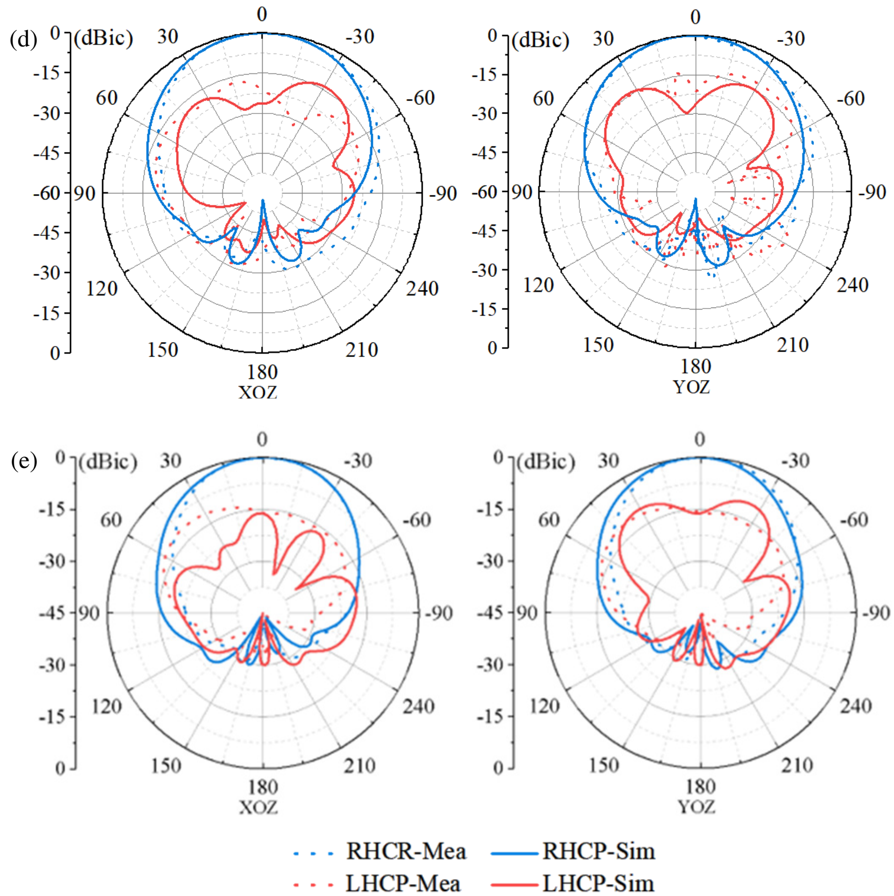

FIGURE 10. Simulation and measurement results of radiation patterns at (a) 2.5 GHz, (b) 3 GHz, (c) 3.5 GHz, (d) 4 GHz, and (e) 4.3 GHz.

measurement data, was calculated to be over 88% across the band.

The radiation patterns in the two principal planes (E-plane: XOZ, H-plane: YOZ) were measured at five representative frequencies: 2.5 GHz, 3.0 GHz, 3.5 GHz, 4 GHz, and 4.3 GHz, as shown in Fig. 10. Evidently, both the co-polarization (RHCP) and cross-polarization (LHCP) components remain at significantly low levels across a wide angular range in the back direction, not merely at a single point ($\theta = 180°$). This demonstrates that the proposed tilted-slot fences, in conjunction with the cavity structure, provide broadband and wide-angle suppression of backward radiation. Furthermore, the low LHCP level in the rear hemisphere confirms that the backward radiation is suppressed without degrading the polarization purity of the main forward beam. The measured patterns align well with the simulated trends, confirming the robustness of the proposed design.

To address the advantages of our proposed work, Table 1 compares the relevant work. As shown, the proposed work demonstrates significant advantages across multiple core specifications: It achieves a 3 dB AR bandwidth of 54%, notably wider than most counterparts. Wideband high FBR is achieved around 27.5 dB, outperforming the best value among the cited works by approximately 7.5 dB, which highlights the exceptional effectiveness of the novel tilted-slot fences in suppressing backward radiation.

4. CONCLUSION

A wideband CP antenna with a significantly enhanced FBR has been proposed, achieved through the synergistic integration of a grooved loop resonator and a parasitic zigzag patch for broadband AR performance, and combined with a cavity-backed structure employing tilted slot fences to achieve a stable FBR of around 27.5 dB. Compared to traditional directional CP antennas, the FBR of the proposed design has been improved by more than 10 dB. The fabricated antenna exhibits an 85.5% impedance bandwidth, a 54% 3 dB AR bandwidth, and a peak gain of 9.3 dBic. Its fully planar, PCB-compatible design offers a cost-effective and practical solution for applications requiring high gain and enhanced FBR unidirectional circular polarization.

ACKNOWLEDGEMENT

This work was supported in part by the State Key Laboratory of Millimeter Waves under Grant K202535, in part by the Guangzhou Basic and Applied Basic Research Subject (Young Doctor "Sailing" project) under Grant 2024A04J3689, and in part by the National Natural Science Foundation of China under Grant 61901176.

REFERENCES

[1] Wu, R., J.-H. Lin, G.-H. Wen, S.-T. Cai, and F.-C. Chen, "A compact broadband circularly polarized antenna with novel tilt fences for GNSS applications," *IEEE Antennas and Wireless Propagation Letters*, Vol. 23, No. 5, 1528–1532, May 2024.

[2] Yang, W., Y. Pan, S. Zheng, and P. Hu, "A low-profile wideband circularly polarized crossed-dipole antenna," *IEEE Antennas and Wireless Propagation Letters*, Vol. 16, 2126–2129, 2017.

[3] Yang, W.-J., Y.-M. Pan, and S.-Y. Zheng, "A compact broadband circularly polarized crossed-dipole antenna with a very low profile," *IEEE Antennas and Wireless Propagation Letters*, Vol. 18, No. 10, 2130–2134, Oct. 2019.

[4] Kumar, K., S. Dwari, and M. K. Mandal, "Dual-band dual-sense circularly polarized substrate integrated waveguide antenna," *IEEE Antennas and Wireless Propagation Letters*, Vol. 17, No. 3, 521–524, Mar. 2018.

[5] Baik, J.-W., K.-J. Lee, W.-S. Yoon, T.-H. Lee, and Y.-S. Kim, "Circularly polarised printed crossed dipole antennas with broadband axial ratio," *Electronics Letters*, Vol. 44, No. 13, 785–786, 2008.

[6] Baik, J.-W., T.-H. Lee, S. Pyo, S.-M. Han, J. Jeong, and Y.-S. Kim, "Broadband circularly polarized crossed dipole with parasitic loop resonators and its arrays," *IEEE Transactions on Antennas and Propagation*, Vol. 59, No. 1, 80–88, Jan. 2011.

[7] He, Y., W. He, and H. Wong, "A wideband circularly polarized cross-dipole antenna," *IEEE Antennas and Wireless Propagation Letters*, Vol. 13, 67–70, 2014.

[8] Guo, L. and K. W. Leung, "Compact linearly and circularly polarized unidirectional dielectric resonator antennas," *IEEE Transactions on Antennas and Propagation*, Vol. 64, No. 6, 2067–2074, Jun. 2016.

[9] Wu, R., J.-H. Lin, J.-F. Li, and F.-C. Chen, "Wideband circularly polarized antenna with novel asymmetric Y-shaped arms," *IEEE Antennas and Wireless Propagation Letters*, Vol. 23, No. 4, 1181–1185, Apr. 2024.

[10] Li, D., L. Li, Z. Li, and G. Ou, "Four-arm spiral antenna fed by tapered transmission line," *IEEE Antennas and Wireless Propagation Letters*, Vol. 16, 62–65, 2017.

[11] Mehrabani, A. and L. Shafai, "Compact dual circularly polarized primary feeds for symmetric parabolic reflector antennas," *IEEE Antennas and Wireless Propagation Letters*, Vol. 15, 922–925, 2016.

[12] Radway, M. J. and D. S. Filipovic, "Four-armed spiral-helix antenna," *IEEE Antennas and Wireless Propagation Letters*, Vol. 11, 338–341, 2012.

[13] Tan, M. N. M., M. T. Ali, S. Subahir, T. A. Rahman, and S. K. A. Rahim, "Backlobe reduction using mushroom-like EBG structure," in *2012 IEEE Symposium on Wireless Technology and Applications (ISWTA)*, 206–209, Bandung, Indonesia, 2012.

[14] Zheng, P., Y. Qiu, J. Bai, Z. Xu, X. Liu, J. Liu, J. Li, S. Zhang, H. Zhu, and G. Wei, "Broadband dual-polarized antenna with enhanced front-to-back ratio using metasurface," in *2019 IEEE Asia-Pacific Microwave Conference (APMC)*, 1742–1744, Singapore, 2019.

[15] Peng, L., J.-Y. Xie, X.-F. Li, and X. Jiang, "Front to back ratio bandwidth enhancement of resonance based reflector antenna by using a ring-shape director and its time-domain analysis," *IEEE Access*, Vol. 5, 15 318–15 325, 2017.

[16] Govindanarayanan, I. and N. Rangaswamy, "Asymmetric folded dipole antenna with high front-to-back ratio for LTE base stations," *IEEE Antennas and Wireless Propagation Letters*, Vol. 15, 869–872, 2016.

[17] Liang, Z., C. Lu, Y. Li, J. Liu, and Y. Long, "A broadband dual-polarized antenna with front-to-back ratio enhancement using semicylindrical sidewalls," *IEEE Transactions on Antennas and Propagation*, Vol. 66, No. 7, 3735–3740, Jul. 2018.

[18] Zhang, L., S. Gao, Q. Luo, P. R. Young, Q. Li, Y.-L. Geng, and R. A. Abd-Alhameed, "Single-feed ultra-wideband circularly polarized antenna with enhanced front-to-back ratio," *IEEE Transactions on Antennas and Propagation*, Vol. 64, No. 1, 355–360, Jan. 2016.

[19] Song, S. and X. Chen, "A compact and broadband dielectric resonator magnetoelectric dipole antenna with high front-to-back ratio," *IEEE Antennas and Wireless Propagation Letters*, Vol. 23, No. 1, 239–243, Jan. 2024.

[20] Li, R., Y. Huang, J. Du, and Y. Cui, "Front-to-back ratio improvement of a compact base-station antenna for 5G NR applications," *Microwave and Optical Technology Letters*, Vol. 66, No. 2, e34063, 2024.

[21] Rao, S.-L., Q.-M. Cai, X. Cao, L. Tao, A. Huang, M. Liu, Y. Zhu, Y. Zhu, P. Bo, Y. Yu, and J. Fan, "Front-to-back ratio and half-power beamwidth improving for 4G/5G base station antenna," *IET Microwaves, Antennas & Propagation*, Vol. 16, No. 15, 955–961, 2022.

[22] An, N. and Y. Zhang, "Dual-band dual-sense circularly polarized antenna utilizing a radiating slot antenna as feeding structure," *IEEE Antennas and Wireless Propagation Letters*, Vol. 23, No. 4, 1321–1325, Apr. 2024.

[23] Mao, C., M. Khalily, R. Tafazolli, and A. Kishk, "Wideband dual circularly polarized helical antenna array for satellite applications," *IEEE Antennas and Wireless Propagation Letters*, Vol. 23, No. 9, 2758–2762, Sep. 2024.

[24] Yang, W. J., P. F. Hu, and X. Dai, "A filtering, wideband circularly polarized crossed-dipole antenna," *IEEE Transactions on Antennas and Propagation*, Vol. 73, No. 11, 9583–9588, Nov. 2025.

[25] Gu, W. D. and Y. Zhang, "A type of dual/circularly polarized filtering dipole antenna design based on coupled lines," *IEEE Antennas and Wireless Propagation Letters*, Vol. 24, No. 2, 489–493, Feb. 2025.